RSC Advances

PAPER

View Article Online
View Journal | View Issue

Cite this: *RSC Adv.*, 2024, **14**, 21991

MgAl-LDH nanoflowers as a novel sensing material for high-performance humidity sensing†

Luyu Wang, *[a] Jia Song[b] and Chunyang Yu[c]

Received 23rd May 2024
Accepted 3rd July 2024

DOI: 10.1039/d4ra03800b

rsc.li/rsc-advances

This work details a novel application of MgAl-LDH nanoflowers, applied in the fabrication of humidity sensors using quartz crystal microbalance (QCM). An oscillating circuit approach has been utilized to thoroughly investigate the humidity detection characteristics of QCM sensors that are fabricated using MgAl-LDH nanoflowers. The examination encompassed various parameters such as the sensors' response, humidity hysteresis, repeatability, and stability. Experimental results clearly indicate that these MgAl-LDH nanoflower-based QCM sensors exhibit a distinct logarithmic frequency response to varying moisture levels. Notably, the sensitivity of the sensors is intricately tied to the amount of MgAl-LDH nanoflowers utilized during the deposition process. Moreover, these sensors maintain remarkable stability across a wide humidity range spanning from 11% to 97% RH. Additionally, the MgAl-LDH nanoflower-based QCM sensors possess minimal humidity hysteresis and display swift dynamic response and recovery periods, further highlighting their potential for humidity detection applications.

1 Introduction

Alternately referred to as hydrotalcites, Layered Double Hydroxides (LDHs) encompass a class of inorganic compounds that are uniquely identified by their two-dimensional stratified composition.[1] The crystal structure of LDHs consists of layers of positively charged metal hydroxides, interleaved with interchangeable anions and water molecules located between these layers.[2] In these stratified metal hydroxide layers, certain divalent metal ions (like Mg^{2+}, Zn^{2+}) are often replaced to some extent by trivalent metal ions (such as Al^{3+}, Fe^{3+}), leading to a charge imbalance.[3,4] The imbalance is balanced by the presence of interlayer anions (like Cl^-, NO_3^-, CO_3^{2-}) and water molecules, which play a role in stabilizing the structure.[5,6] Owing to their unique composition and ion-exchange properties, LDHs are extensively utilized in various fields such as catalysis, drug delivery, wastewater treatment, and adsorption, demonstrating their versatility and applicability across diverse applications.[7–10] LDHs can be synthesized using diverse techniques such as co-precipitation, hydrothermal synthesis, and ion exchange. Their functionality can be tailored by adjusting the layered composition, interlayer anions, and conditions of synthesis, offering a high degree of versatility and customization.[11–13]

The magnesium aluminum Layered Double Hydroxide (MgAl-LDH), a category of inorganic substances, is distinguished by its distinct stratified composition, featuring alternating strata of Mg^{2+} and Al^{3+} hydroxides.[14] The proportion between divalent and trivalent metal ions affects its characteristics.[15] Nestled within these strata lie negatively charged anions like CO_3^{2-}, NO_3^-, and Cl^-, exchangeable with cations and water molecules.[16] The configuration of MgAl-LDH is crucial for its exceptional porosity and surface area, enhancing its efficacy and selectivity in diverse applications including environmental pollution management, drug delivery, photocatalysis facilitation, and serving as a catalyst in numerous chemical reactions. These unique properties render MgAl-LDH a valuable material with broad applicability.[17–20] Huang and others discovered the hydrophilic nature of MgAl-LDH,[21] showcasing its capabilities in detecting humidity.

Gas sensors are devices used to detect various gases or humidity in the air.[22–26] In the realm of sensing technology, a quartz crystal microbalance (QCM) transducer serves as a vital component, converting physical changes in the sensor into electrical signals, thus enabling accurate and sensitive detection.[27] The QCM transducer, a well-established platform for mass detection, boasts remarkable sensitivity, capable of identifying mass variations down to the sub-nanogram level, leveraging Sauerbrey's correlation to ensure precise measurements.[28] Drawing upon Sauerbrey's correlation, the QCM transducer effectively transforms the absorbed molecular mass into a frequency-sensitive signal by applying sensing substances

[a]College of Artificial Intelligence and E-Commerce, Zhejiang Gongshang University Hangzhou College of Commerce, Hangzhou, 311599, China. E-mail: Dr.Luyu-Wang@hotmail.com

[b]School of Nuclear Science and Engineering, Shanghai Jiao Tong University, Shanghai, 200240, China. E-mail: songjia111@sjtu.edu.cn

[c]Design-AI Laboratory, China Academy of Art, Hangzhou 310009, China. E-mail: yucyzju@hotmail.com

† Electronic supplementary information (ESI) available: The chemical raw materials and synthesis method of MgAl-LDH nanoflowers; characterization; fabrication and test methods of the QCM humidity sensor; schematic of the humidity testing system. See DOI: https://doi.org/10.1039/d4ra03800b

Table 1 Comparison between QCM based humidity sensors in reported work and this work

Material	Detection limit	Response	Response time	Reference
rGO/PEO	11%	~200 Hz	11 s	34
GO/PEI	32%	~600 Hz	53 s	35
F^- doping MXene	11%	<400 HZ	6 s	36
HKUST-1	22%	720 Hz	116 s	37
$ZnCo_2O_4$/polypyrrole	11%	~250 Hz	8 s	38
MgAl-LDH nanoflowers	11%	485 Hz	9 s	This paper

onto its electrodes, thus enabling sensitive and accurate detection.[29] Lately, an increasing number of scientists are investigating the application of QCM transducers in creating humidity sensors.[30,31] Although there are currently reports on MgAl-LDH modified QCM,[32,33] its application focuses on monitoring ion dynamic behavior, and there is no humidity sensor related application. In this work, the humidity detection capabilities of MgAl-LDH nanoflowers are examined using a QCM transducer. Experimental evaluation of the MgAl-LDH nanoflowers based QCM sensors' ability to detect humidity involves assessing their frequency response, moisture hysteresis, repeatability, stability, and selectivity. As shown in Table 1, this sensor does not exhibit significant performance disadvantages compared to several previously reported humidity sensors, highlighting the innovative application direction of MgAl-LDH nanoflowers in humidity sensor technology.

2 Experimental section

2.1. The chemical raw materials and devices

Details on the chemical substances employed in the synthesis of MgAl-LDH nanoflowers can be found in the ESI.† Chengdu Westarace Electronic Co., China, supplied the QCM chip, adorned with silver electrode coating. Each QCM resonator is set to a standard frequency of 10^7 Hz (AT-cut).

2.2. Synthesis of MgAl-LDH nanoflowers

An in-depth explanation of the MgAl-LDH nanoflowers synthesis process is provided in the ESI section.†

2.3. Characterization, fabrication and test methods of the QCM humidity sensor

Details on the instruments and methods employed for the characterization of MgAl-LDH nanoflowers can be found in the ESI.†

Detailed descriptions of the production and examination techniques for the MgAl-LDH nanoflowers based QCM humidity sensor are provided in the ESI.† The sketch diagram of humidity detection system is illustrated in Fig. S1 of the ESI.† To assess how the amount of MgAl-LDH nanoflowers deposited impacts sensor efficiency, sensors containing 1, 2, and 3 μL of MgAl-LDH nanoflowers dispersion on QCMs' electrodes were constructed. The corresponding sensors were designated as QCM-1, QCM-2, and QCM-3. The specific information of the QCM samples before and after MgAl-LDH nanoflowers deposition, including frequency, crystal's resistance ($R_{crystal}$), *etc.*, is shown in Table 2.

3 Results and discussion

3.1. Materials characterization

Wide angle X-ray diffraction (XRD) spectra for MgAl-LDH nanoflowers were gathered to ascertain the crystal structure and potential phase alterations during the preparation process, as depicted in Fig. 1a. The usual high peaks of MgAl-LDH (JCPDS 54-1030) at (003), (006), (012), (009), (018), (110) and (113) planes were noticeable, signifying effective synthesis.[39] Fig. 1b displays the FT-IR spectral data for MgAl-LDH nanoflowers. The spectral absorption near 3440 cm^{-1} in MgAl-LDH nanoflowers is attributable to the elongation vibration in the hydroxyl groups of LDHs layers. The observed peak at 1622 cm^{-1} is attributable to the bending vibration of H_2O. The distinct band observed at 1354 cm^{-1} could result from NO_3^- contamination during the creation of MgAl-LDH nanoflowers.[40] Furthermore, the observed peaks at 751 cm^{-1} and 449 cm^{-1} result from the lattice oscillations of M–O and M–O–M (M = Mg, Al), aligning with prior studies.[41]

The structural and dimensional characteristics of the MgAl-LDH nanoflowers were thoroughly analyzed using scanning electron microscope (SEM) imaging. As shown in Fig. 2a and b,

Table 2 List of QCM information before and after MgAl-LDH nanoflowers deposition

	Bare QCM sensor (before MgAl-LDH nanoflowers deposition)		QCM sensor after MgAl-LDH nanoflowers deposition		Frequency and $R_{crystal}$ shifts due to MgAl-LDH nanoflowers deposition		Deposition mass of MgAl-LDH nanoflowers (ng)
Sample number	Frequency (Hz)	$R_{crystal}$ (Ω)	Frequency (Hz)	$R_{crystal}$ (Ω)	Δf (Hz)	$\Delta R_{crystal}$ (Ω)	
QCM-1	9 985 878	5.427862	9 985 473	5.606280	405	0.178418	210.9375
QCM-2	9 985 911	5.591627	9 984 994	6.131448	917	0.539821	477.6042
QCM-3	9 985 892	5.398821	9 984 633	8.787252	1259	3.38843	655.7296

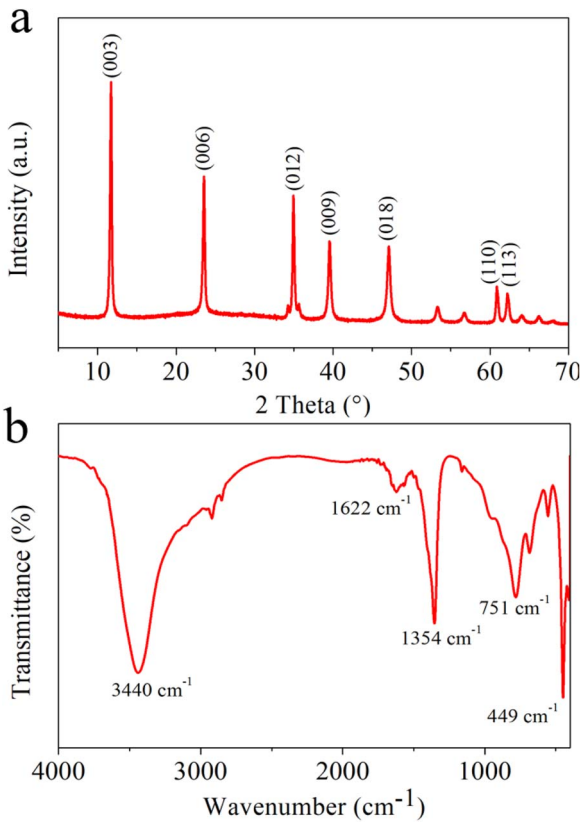

Fig. 1 (a) XRD pattern of MgAl-LDH nanoflowers. (b) FT-IR spectra of MgAl-LDH nanoflowers.

the SEM photographs reveal that the MgAl-LDH nanoflowers exhibit a clustered formation, resembling the shape of rose petals, with a distinct planar sheet morphology. The nanoflowers exhibit both dispersive and fluffy properties, highlighting their unique structure. Furthermore, transmission electron microscopy (TEM) images, depicted in Fig. 2c and d, reveal a level of transparency in the nanosheets of the MgAl-LDH nanoflowers, indicating their remarkably thin thickness. This observation further confirms the unique and delicate structure of these nanoflowers.

The SEM image of single MgAl-LDH nanoflower together with selected-area element analysis maps of O, Mg, and Al in Fig. 3a indicates that all O (red), Mg (green), and Al (cyan) atoms are distributed uniformly through the whole selected-area, revealing a homogeneous distribution of O, Mg, and Al in the structure of MgAl-LDH nanoflowers. This MgAl-LDH nanoflower was additionally employed in the point analyses of energy dispersive spectra (EDS) (refer to Fig. 3b), illustrating the simultaneous presence of O, Mg, and Al atoms dispersed across the MgAl-LDH nanoflower surface. The comprehensive composition of MgAl-LDH nanoflower was determined through inductively coupled plasma atomic emission spectroscopy (ICP-AES) analysis, as depicted in Table 3. The MgAl-LDH nanoflowers exhibit a weight concentration of 50.60% for O, 33.61% for Mg, and 15.79% for Al, as determined through precise compositional analysis.

To evaluate the influence of varying MgAl-LDH nanoflower deposition amounts on sensor efficiency, we fabricated sensors

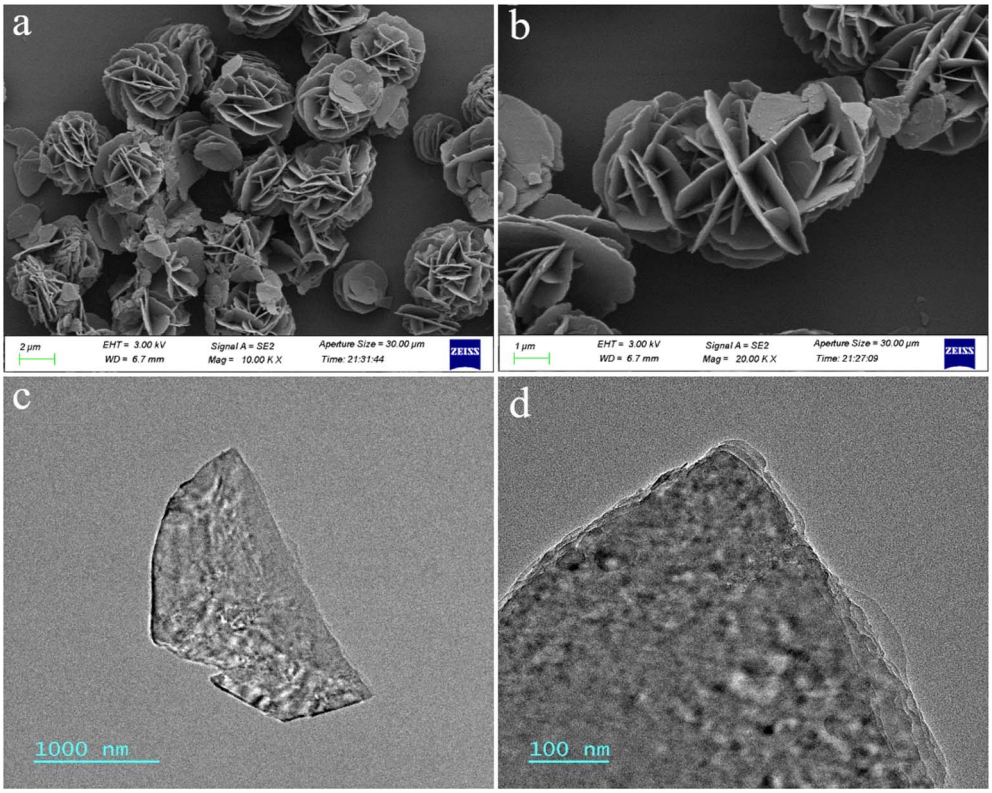

Fig. 2 (a) and (b) SEM images of MgAl-LDH nanoflowers. (c) and (d) TEM images of MgAl-LDH nanoflowers.

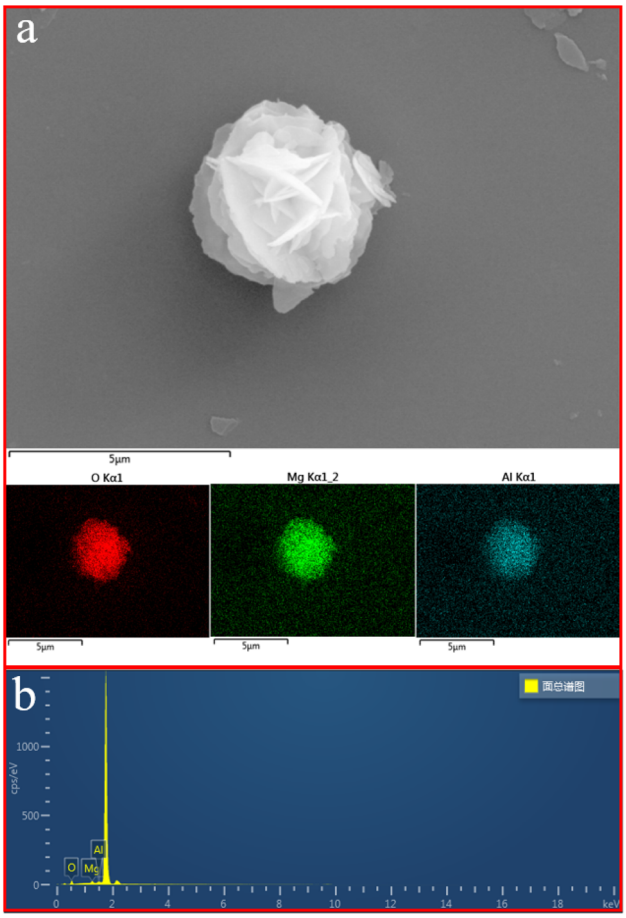

Fig. 3 (a) Elemental mapping characterization of prepared MgAl-LDH nanoflower. (b) EDS profile obtained from MgAl-LDH nanoflower.

Table 3 Relative compositions of O, Mg, and Al atoms obtained from ICP-AES analysis

Element	Amount (wt%)
O	50.60
Mg	33.61
Al	15.79

with precisely 1, 2, and 3 μL of MgAl-LDH nanoflower dispersion deposited onto the electrodes of QCMs. These tailored sensors were designated as QCM-1, QCM-2, and QCM-3, respectively. Surface structures of QCM-1, QCM-2, and QCM-3 were examined using SEM. As depicted in Fig. 4a–c, it's noticeable that with the addition of more MgAl-LDH nanoflowers disperse liquid, there's a corresponding rise in the distribution density of MgAl-LDH nanoflowers. Concurrently, as depicted in Fig. 4d–f, surface water droplet contact angles were tested on QCM-1, QCM-2, and QCM-3 at angles of 69.39°, 69.57°, and 69.80°, respectively. As is commonly known, a water droplet's contact angle below 90° indicates a hydrophilic surface.[42] This suggests that the surfaces of the three sensors are hydrophilic, thereby enabling them to detect humidity effectively.

3.2. Humidity sensing properties

The capacity of MgAl-LDH nanoflower based QCM sensors to detect humidity was evaluated by modulating the relative humidity and subsequently recording the corresponding frequency shift. Fig. 5a portrays the variation in frequency exhibited by these MgAl-LDH nanoflower based QCM sensors as a function of the relative humidity. This illustration conspicuously demonstrates a decline in frequency as humidity levels increase across all three sensor types. Specifically, as humidity varies from 11% to 97%, the frequency shifts to −1747 Hz, −2019 Hz, and −4085 Hz for the QCM-1, QCM-2, and QCM-3 sensors, respectively. This indicates a significant correlation between the frequency alteration in MgAl-LDH nanoflowers based QCM sensors and the quantity of MgAl-LDH nanoflowers deposited. Among the trio of sensors, the QCM-3 sensor exhibits the most pronounced frequency shift in response to a given humidity variation. This enhanced sensitivity to humidity in the QCM-3 sensor stems from the increased availability of water absorption sites, a consequence of the higher concentration of MgAl-LDH nanoflowers utilized. Additionally, it's noticeable that the frequency shift trajectories for each of the three sensors display a logarithmic correlation. The BET model adsorption theory accounts for this rare occurrence.[43] Water vapor is adsorbed onto the surface of MgAl-LDH nanoflowers, a process known as multi-molecular-layer adsorption. The BET model suggests that the quantity of water vapor absorbed by the QCM under varying relative humidity levels approaches a logarithmic correlation. This results in a logarithmic relationship between the frequency shift and the corresponding relative humidity. The logarithmic fitting outcome for these response curves is shown in Fig. 5b. For the QCM-1, QCM-2, and QCM-3 sensors, the regression coefficients, R^2, stand at 0.99759, 0.98504, and 0.99008, respectively. Consequently, QCM sensors based on MgAl-LDH nanoflowers demonstrate a distinct logarithmic reaction in relation to humidity.

Hysteresis levels play a crucial role in humidity sensing, and minimizing them is highly desirable.[44] To evaluate the hysteresis in MgAl-LDH nanoflower-based QCM sensors, the sensors were subjected to a humidity cycle, initially increasing from 11% to 97% RH for water absorption, and subsequently decreasing to 11% RH for water desorption. Fig. 6 illustrates the ensuing curves of humidity hysteresis. This illustration reveals that the desorption response curves of the MgAl-LDH nanoflower based QCM sensors lag slightly behind their adsorption response curves. Across the full spectrum of humidity (11–97% RH), the MgAl-LDH nanoflowers based QCM sensors exhibit no noticeable humidity hysteresis. The minimal humidity hysteresis noted is due to the enhanced adsorption and desorption of water molecules in MgAl-LDH nanoflowers. The two-dimensional structural characteristics and numerous active sites present in MgAl-LDH nanoflowers offer significant advantages for the adsorption and desorption of water molecules.

Lucklum *et al.* found that an increase in frequency in QCM is accompanied by an increase in its resistance, and excessive

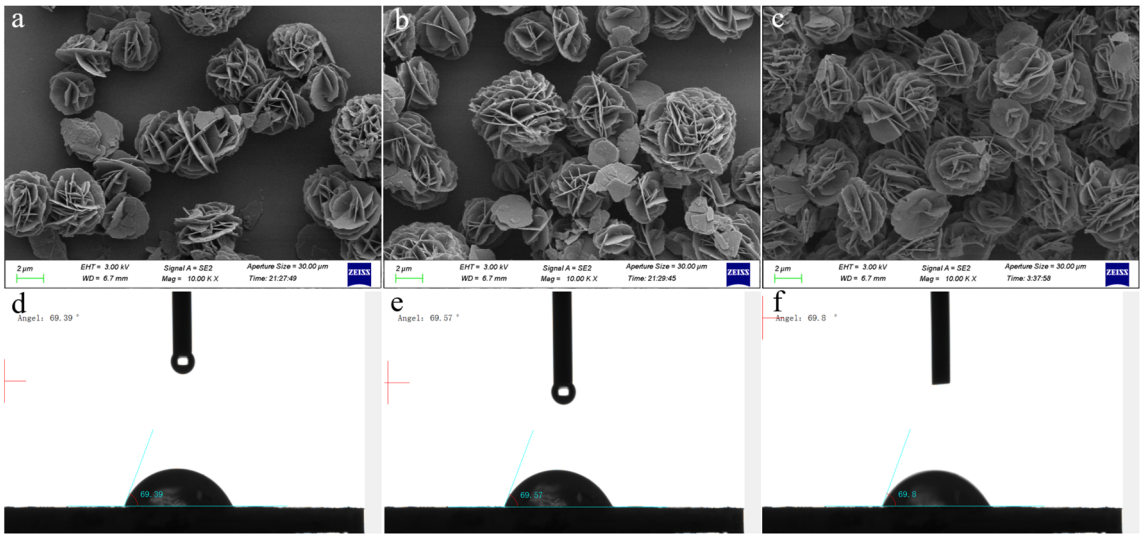

Fig. 4 Surficial SEM images of (a) QCM-1, (b) QCM-2, and (c) QCM-3. The contact angle test result of (d) QCM-1, (e) QCM-2, and (f) QCM-3.

frequency is detrimental to the stability of the QCM.[45] Additionally, Vig *et al.* reported that resistance is proportional to the energy dissipation of a quartz resonator, and excessive energy dissipation is detrimental to the stability of the quartz resonator.[46] Therefore, a larger resistance results in a poorer stability of a QCM.[43] The variation in the crystal's resistance ($R_{crystal}$) of the MgAl-LDH nanoflowers based QCM sensors to

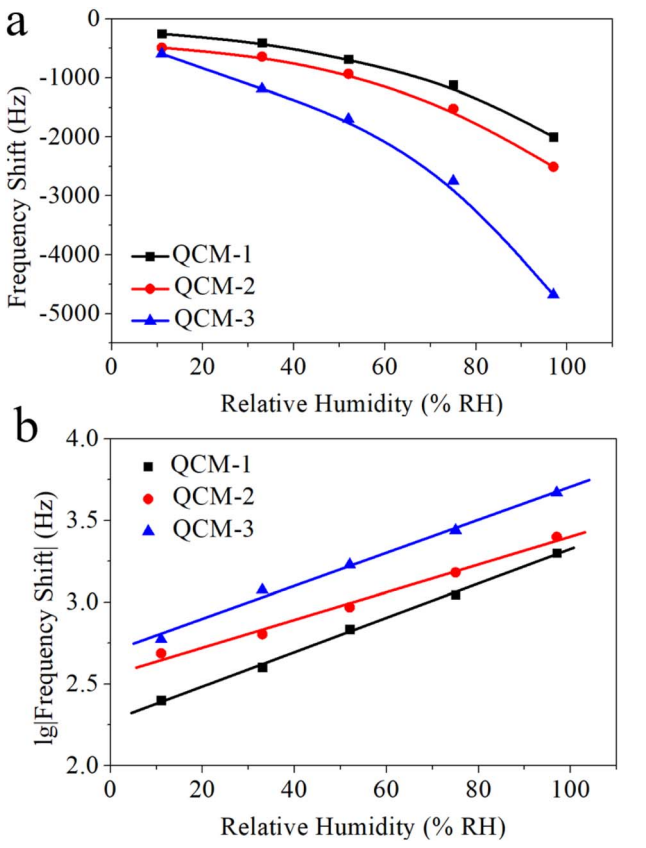

Fig. 5 (a) The frequency shift data of QCM-1, QCM-2, and QCM-3 as a function of humidity. (b) The logarithmic fitting curves of log(frequency shift) *versus* humidity for QCM-1, QCM-2, and QCM-3.

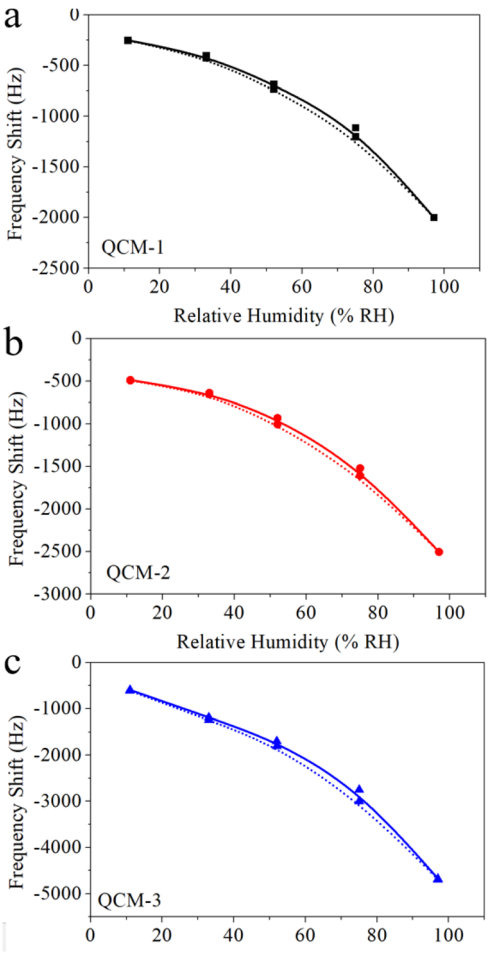

Fig. 6 Humidity hysteresis curves of (a) QCM-1, (b) QCM-2, and (c) QCM-3.

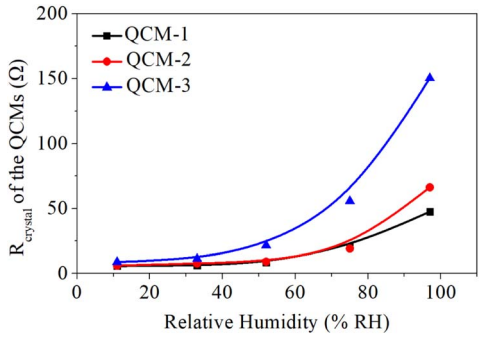

Fig. 7 The change in $R_{crystal}$ of QCM-1, QCM-2, and QCM-3 as a function of humidity.

humidity levels was observed to assess the sensors' stability. Fig. 7 illustrates the $R_{crystal}$ measurements of sensors under various humidity conditions, noting that the $R_{crystal}$ readings of QCM sensors using MgAl-LDH nanoflowers fall within a 60 Ω range in humidity between 11% and 75% RH. Nonetheless, it's important to mention that the $R_{crystal}$ readings of the sensor, particularly the QCM-3 sensor, which contains numerous MgAl-LDH nanoflowers, showed a significant rise when humidity levels exceeded 75%. As an illustration, the QCM-3 sensor's $R_{crystal}$ measurement stood at 151 at 97% RH, approximately 17 times higher than its measurement at 11.3% RH. The findings suggest that the steadiness of the MgAl-LDH nanoflowers based QCM sensor, when heavily laden with MgAl-LDH nanoflowers, deteriorates in environments with elevated humidity, rendering it ineffective for precise identification of extremely high humidity.[43] Therefore, in practical applications, it's crucial not to blindly increase the quantity of material loaded onto the QCM surface, but rather to choose an appropriate quantity of MgAl-LDH nanoflowers for deposition, which is essential for maintaining a balance between sensitivity and stability. In this study, based on the comprehensive test results from Fig. 5 and 7, QCM-2 was found to have a good balance between sensitivity and resistance stability compared to QCM-1 and QCM-3, so it was selected for further testing.

The response and recovery curve of the QCM-2 sensor demonstrates its sensing characteristics. This curve clearly show how the sensors detect H_2O molecule adsorption and desorption, thereby evaluating their performance in humidity sensing. As shown in Fig. 8a, the QCM-2 sensor shows continuous frequency shift to relative humidity ranging from 11% RH to 97% RH. This sensor demonstrates good reversibility as the relative humidity increases. When the QCM-2 sensor is returned to 0% RH, the baseline quickly re-establishes. Fig. 8b shows the response time and recovery time of the QCM-2 sensor. The response time is the duration for a sensor to achieve 90% of the total frequency change during response, while the recovery time is the duration for a sensor to achieve 90% of the total frequency change during recovery.[47] The response time and recovery time of the QCM-2 sensor are 9 s and 12 s, respectively. To assess the repeatability of the QCM-2 sensor, it was relocated to an 11% RH setting for a trio of cycles. To assess the short-term

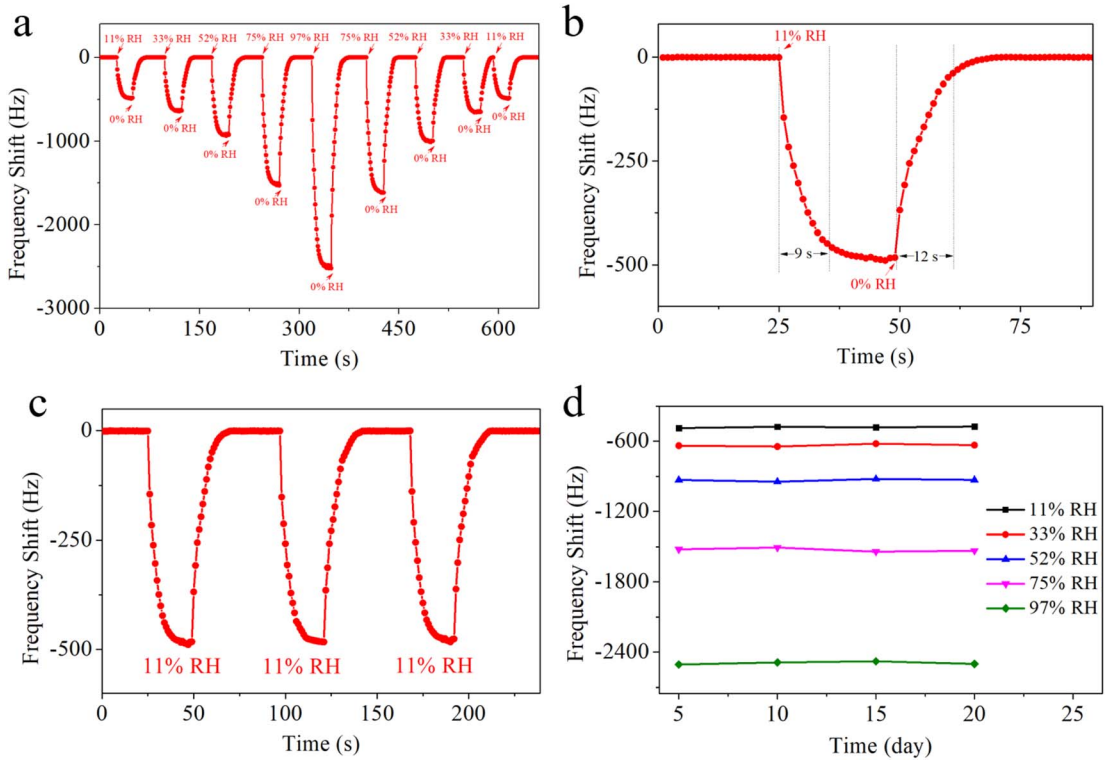

Fig. 8 (a) Dynamic frequency shift of the prepared QCM-2 sensor. (b) The response time and recovery time of the prepared QCM-2 sensor to 11% RH. (c) Repeatability of the QCM-2 sensor for three alternating humidity cycles. (d) Long-term stability of QCM-2 sensor.

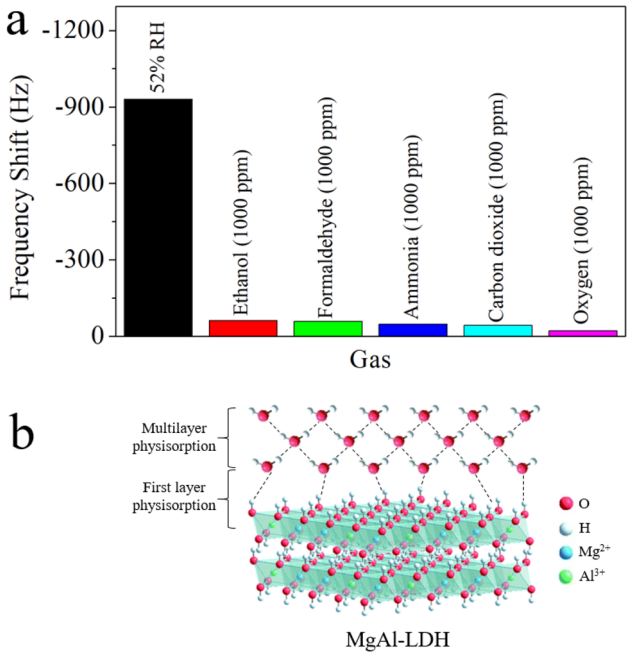

Fig. 9 (a) Selectivity of the QCM-2 sensor towards 52% RH and 1000 ppm various gasses. (b) Schematic of humidity sensing at MgAl-LDH nanoflowers.

repeatability of the QCM-2 sensor, it was relocated to an 11% RH environment for three cycles of testing. As shown in Fig. 8c, the sensor's output frequencies were captured instantaneously throughout the entire process, demonstrating that after three rounds of varying humidity conditions, the frequency of the QCM-2 sensor consistently reverted to its original level, highlighting its short-term repeatability. Extensive research has been conducted to assess the long-term stability of the QCM-2 sensor. As depicted in Fig. 8d, the QCM-2 sensor underwent weekly testing across various relative humidity levels (11%, 33%, 52%, 75%, and 97%) for a duration of 20 days, demonstrating consistent stability without any significant changes over time.

Fig. 9a illustrates the sensitivity of QCM-2 sensor to 52% RH and 1000 ppm concentrations of various gases, including ethanol, formaldehyde, ammonia, carbon dioxide, and oxygen. Evidently, when contrasted with the 1000 ppm interference gases, the QCM-2 sensor exhibited a significantly greater frequency shift towards water molecules. Evidence shows the humidity sensor's high specificity towards water molecules. This remarkable selectivity can be attributed to the abundant hydroxyl groups on the surface of MgAl-LDH nanoflowers.[48] Many scientists have already reported the reversible adsorption and desorption capabilities of hydroxyl groups for water molecules in the air, as hydrogen bonding adsorption belongs to weak adsorption interaction.[49–51] As shown in Fig. 9b, under humidity conditions, water molecules adhere to the hydroxyl groups, forming an initial adsorption layer *via* hydrogen bonds.[52] As humidity levels increase, water molecules attach to two adjacent hydroxyl groups *via* hydrogen bonds, forming multilayer physisorption water.[53] When environmental humidity decreases sharply, adsorbed water molecules desorb to achieve equilibrium with the surroundings.[54] Additionally, materials with porous structures facilitate the rapid adsorption and desorption of water molecules.[47,55,56]

4 Conclusion

In summary, our comprehensive analysis has centered on exploring the moisture detection capabilities of MgAl-LDH nanoflowers when incorporated into QCM transducers. The QCM sensor, utilizing MgAl-LDH nanoflowers, has exhibited exceptional sensitivity, short response and recovery times, minimal hysteresis, robust long-term stability, and excellent selectivity within the 11–97% RH range. These findings suggest that MgAl-LDH nanoflowers possess significant potential for applications in humidity detection.

Conflicts of interest

The authors declare that they have no known competing financial interests or personal relationships that could have appeared to influence the work reported in this paper.

Acknowledgements

This research was supported by National Natural Science Foundation of China under Grant No. 62001420, Zhejiang Provincial Natural Science Foundation of China under Grant No. LQ21F010017, University-Industry Collaborative Education Program under Grant No. 220400576262052, and Science Foundation of Zhejiang Gongshang University Hangzhou College of Commerce, Zhejiang Gongshang University, China (ZJHZCC) under Grant No. 2222111.

References

1 Z. Wang, W. A. Goddard III and H. Xiao, *Nat. Commun.*, 2023, **14**, 4228.
2 T. He, Q. Li, T. Lin, J. Li, S. Bai, S. An, X. Kong and Y.-F. Song, *Chem. Eng. J.*, 2023, **462**, 142041.
3 M. L. Jadam, S. H. Sarijo and Z. Jubri, *Mater. Today: Proc.*, 2022, **66**, 4015–4019.
4 X.-J. Zhao, S.-M. Xu, Y. Zhong, Z.-R. Chen, P. Yin, Y.-C. Miao, J.-Y. Guo, W. Zhang, Y. Jie and H. Yan, *J. Phys. Chem. C*, 2022, **126**, 1356–1365.
5 S. A. Zakaria, S. H. Ahmadi and M. H. Amini, *Sens. Actuators, A*, 2022, **346**, 113827.
6 Q. Wang and D. O'Hare, *Chem. Rev.*, 2012, **112**, 4124–4155.
7 K. Karadi, T.-T. Nguyen, A. A. Adam, K. Baan, A. Sapi, A. Kukovecz, Z. Konya, P. Sipos, I. Palinko and G. Varga, *Green Chem.*, 2023, **25**, 5741–5755.
8 S. Bahraminejad, A. Pardakhty, I. Sharifi, A. Keyhani, E. Salarkia and M. Ranjbar, *Heliyon*, 2023, **9**, e15308.
9 Q. Xu, Z. Yue, R. Deng, X. Wang, X. He, X. Chuai, S. Wang and J. Wang, *J. Water Process Eng.*, 2023, **56**, 104270.
10 M. Zheng, J. Wang, D. Fu, B. Ren, X. Song, K. Kan and X. Zhang, *J. Hazard. Mater.*, 2023, **442**, 130068.

11 A. Farhan, A. Khalid, N. Maqsood, S. Iftekhar, H. M. A. Sharif, F. Qi, M. Sillanpaa and M. B. Asif, *Sci. Total Environ.*, 2024, **912**, 169160.
12 S. Li, J. Lu, M. Wei, D. G. Evans and X. Duan, *Adv. Funct. Mater.*, 2010, **20**, 2848–2856.
13 F. Li, Z. Sun, H. Jiang, Z. Ma, Q. Wang and F. Qu, *Energy Fuels*, 2020, **34**, 11628–11636.
14 N. Iyi, Y. Ebina and T. Sasaki, *Langmuir*, 2008, **24**, 5591–5598.
15 D. Liang, W. Yue, G. Sun, D. Zheng, K. Ooi and X. Yang, *Langmuir*, 2015, **31**, 12464–12471.
16 Q. Li, Z. Wu, S. Bai, Y. Liu, J. Li and Y.-F. Song, *Chem.–Eur. J.*, 2023, **29**, e202300050.
17 Y. Li, M. Wu, J. Wu, Y. Wang, Z. Zheng and Z. Jiang, *Sep. Purif. Technol.*, 2022, **297**, 121484.
18 S. Sohrabnezhad, Z. Poursafar and A. Asadollahi, *Appl. Clay Sci.*, 2020, **190**, 105586.
19 P. Zhu, M. Gao, J. Zhang, Z. Wu, R. Wang, Y. Wang, E. R. Waclawik and Z. Zheng, *Appl. Catal., B*, 2021, **283**, 119640.
20 K. Yan, Y. Liu, Y. Lu, J. Chai and L. Sun, *Catal. Sci. Technol.*, 2017, **7**, 1622–1645.
21 M. Huang, G. Lu, J. Pu and Y. Qiang, *J. Ind. Eng. Chem.*, 2021, **103**, 154–164.
22 D. Wang, D. Zhang, P. Li, Z. Yang, Q. Mi and L. Yu, *Nano-Micro Lett.*, 2021, **13**, 57.
23 H. Zhang, D. Zhang, R. Mao, L. Zhou, C. Yang, Y. Wu, Y. Liu and Y. Ji, *Nano Energy*, 2024, **127**, 109753.
24 H. Zhang, X. Chen, Y. Liu, C. Yang, W. Liu, M. Qi and D. Zhang, *ACS Appl. Mater. Interfaces*, 2024, **16**, 2554–2563.
25 Y. Zhang, D. Zhang, X. Liu, Y. Yao, M. Tang, H. Zhang and G. Xi, *Sens. Actuators, B*, 2024, **410**, 135643.
26 H. Zhang, D. Zhang, B. Zhang, D. Wang and M. Tang, *ACS Appl. Mater. Interfaces*, 2022, **14**, 48907–48916.
27 J. Du, F. Xie, C. Liu, B. Ji, W. Wei, M. Wang and Z. Xia, *Talanta*, 2023, **259**, 124496.
28 W. Pan, X. Huang, Y. Yao, Q. Chen and D. Liu, *Anal. Chem.*, 2023, **95**, 3075–3081.
29 L. Wang, J. Song and C. Yu, *Microchem. J.*, 2024, **199**, 109967.
30 P. P. Conti, P. Iacomi, M. Nicolas, G. Maurin and S. Devautour-Vinot, *ACS Appl. Mater. Interfaces*, 2023, **15**, 33675–33681.
31 D. Zhang, R. Mao, X. Song, D. Wang, H. Zhang, H. Xia, Y. Ma and Y. Gao, *Sens. Actuators, B*, 2023, **374**, 132824.
32 S. Aisawa, J. Sang, Y. Nitanai, H. Hirahara and E. Narita, *J. Ceram. Soc. Jpn.*, 2021, **129**, 470–477.
33 X. Tan, Z. Jiang, W. Ding, M. Zhang and Y. Huang, *Water Res.*, 2023, **230**, 119558.
34 S. Wang, G. Xie, Y. Su, L. Su, Q. Zhang, H. Du, H. Tai and Y. Jiang, *Sens. Actuators, B*, 2018, **255**, 2203–2210.
35 Z. Yuan, H. Tai, Z. Ye, C. Liu, G. Xie, X. Du and Y. Jiang, *Sens. Actuators, B*, 2016, **234**, 145–154.
36 R. Li, Y. Fan, Z. Ma, D. Zhang, Y. Liu and J. Xu, *Microchim. Acta*, 2021, **188**, 81.
37 L. Kosuru, A. Bouchaala, N. Jaber and M. I. Younis, *J. Sens.*, 2016, **2016**, 4902790.
38 D. Zhang, H. Chen, X. Zhou, D. Wang, Y. Jin and S. Yu, *Sens. Actuators, A*, 2019, **295**, 687–695.
39 R. Shan, L. Yan, K. Yang, Y. Hao and B. Du, *J. Hazard. Mater.*, 2015, **299**, 42–49.
40 J. Li, H. Cui, X. Song, G. Zhang, X. Wang, Q. Song, N. Wei and J. Tian, *RSC Adv.*, 2016, **6**, 92402–92410.
41 Z. P. Xu, G. Stevenson, C.-Q. Lu and G. Q. Lu, *J. Phys. Chem. B*, 2006, **110**, 16923–16929.
42 D. Ahmad, I. van den Boogaert, J. Miller, R. Presswell and H. Jouhara, *Energy Sources, Part A*, 2018, **40**, 2686–2725.
43 Y. Yao, H. Zhang, J. Sun, W. Ma, L. Li, W. Li and J. Du, *Sens. Actuators, B*, 2017, **244**, 259–264.
44 H. Chen, D. Zhang, Q. Pan and X. Song, *IEEE Sens. J.*, 2021, **21**, 4385–4390.
45 R. Lucklum and P. Hauptmann, *Electrochim. Acta*, 2000, **45**, 3907–3916.
46 J. R. Vig, F. L. Walls and IEEE, *Proc. 2000 IEEE/EIA Int. Freq. Control Symp. Exhib.*, IEEE, 2000, pp. 30–33.
47 L. Wang, J. Xu, X. Wang, Z. Cheng and J. Xu, *Sens. Actuators, B*, 2019, **288**, 289–297.
48 M. Du, W. Ye, W. Lv, H. Fu and Q. Zheng, *Eur. Polym. J.*, 2014, **61**, 300–308.
49 L. Tang, W. Chen, B. Chen, R. Lv, X. Zheng, C. Rong, B. Lu and B. Huang, *Sens. Actuators, B*, 2021, **327**, 128944.
50 Q. Fatima, A. A. Haidry, Z. Yao, Y. He, Z. Li, L. Sun and L. Xie, *Nanoscale Adv.*, 2019, **1**, 1319–1330.
51 H. Bi, K. Yin, X. Xie, J. Ji, S. Wan, L. Sun, M. Terrones and M. S. Dresselhaus, *Sci. Rep.*, 2013, **3**, 2714.
52 Z. Chen and C. Lu, *Sens. Lett.*, 2005, **3**, 274–295.
53 F. Temel and I. Ozaytekin, *J. Mater. Sci.: Mater. Electron.*, 2022, **33**, 2801–2815.
54 Q. Chen, Y. Yao, X. Huang, D. Liu and K. Mao, *Sens. Actuators, B*, 2021, **341**, 129992.
55 D. Zhang, H. Chen, P. Li, D. Wang and Z. Yang, *IEEE Sens. J.*, 2019, **19**, 2909–2915.
56 Y. Zhu, H. Yuan, J. Xu, P. Xu and Q. Pan, *Sens. Actuators, B*, 2010, **144**, 164–169.